ECCOMAS Congress 2016
VII European Congress on Computational Methods in Applied Sciences and Engineering
M. Papadrakakis, V. Papadopoulos, G. Stefanou, V. Plevris (eds.)
Crete Island, Greece, 5–10 June 2016

IMAGE SEGMENTATION TECHNIQUES FOR BIOMEDICAL MODELING: ELECTROPHYSIOLOGY AND HEMODYNAMICS

Alexander A. Danilov[1,2], **Roman A. Pryamonosov**[1,2], **and Alexandra S. Yurova**[1,2,3]

[1]Russian Academy of Sciences, Institute of Numerical Mathematics
Gubkina 8, Moscow, 119333, Russia
e-mail: a.a.danilov@gmail.com, breaksound@yandex.ru, sanyka@gmail.com

[2] Moscow Institute of Physics and Technology
Institutskii 9, Dolgoprudny, 141700, Russia

[3] Lomonosov Moscow State University
Leninskie Gory 1, Moscow, 119991, Russia

Keywords: Image Segmentation, Mesh Generation, Medical Images, Hemodynamics, Electrophysiology.

Abstract. *The work addresses segmentation techniques for generation of individualized computational domains on the basis of medical imaging dataset. The computational domains will be used in 3D electrophysiology models and 3D-1D coupled hemodynamics models. Several techniques for user-guided and automated segmentation of soft tissues, segmentation of vascular and tubular structures, generation of centerlines, 1D network reconstruction, correction and local adaptation are examined. We propose two algorithms for automatic vascular network segmentation and user-guided cardiac segmentation.*

1 INTRODUCTION

In this paper we present and develop methods and algorithms for construction of patient-specific discrete geometric models for two important medical applications. Each application imposes specific restrictions on both the input medical images and the output patient-specific discrete model, and, therefore, calls for a specific class of 3D reconstruction methods. The first application considers numerical modelling of hemodynamics. The second application considers electrophysiology modelling.

Individualized regional network of blood vessels is built from patient-specific CT-scans by our fully automatic algorithm for arteries identification. It starts from the fast variant of the isoperimetric distance trees algorithm [1] for aorta identification. The coronary and cerebral networks are reconstructed by the use of Frangi vesselness filter [2]. The filter is based on Hessian 3D analysis of the CT-image and is applicable for all tubular structures in the vascular data set.

Modelling of cardiac electrophysiology may be formalized as the full-scale study of the heart electrical activity from inner-cellular level to the cardiac tissues level. Various mathematical models and numerical methods have been developed for modelling of cardiac electrophysiology [3]. Generally the full-scale electrophysiology modelling involves simulations of electric potential propagation on three different scales: the single-cell models represented by ODE are used on cellular level, the bidomain model represented by PDE system is used on cardiac tissue level, the simplified quasi-static version of Maxwell's equations is used on the whole-body level.

The reconstruction of personalized anatomical model of the pathological heart is one of the crucial steps in electrophysiology modelling. The bidomain model requires an accurate anatomical model of patient heart accounting myocardium anisotropy structure. Our preliminary simulations indicate that electrophysiological processes have low sensitivity to segmentation errors outside the thorax region. Thus, patient-specific segmentation should be focused on the cardiac region, and a reference human model may be used in the remaining part of the body.

The corner stone for medical image processing is segmentation process when each voxel of the 3D medical image is assigned with the particular tissue or internal organ label. Various medical image segmentation techniques have been developed [4, 5, 6]. The most promising fully automatic segmentation methods belong to atlas-based segmentation techniques. The patient-specific segmentation is obtained from the atlas of presegmented images of other individuals. This atlas should contain enough different cases for accurate mapping of the new patient data. Thus atlas-based approach requires huge amount of segmentation expert work for preparation of atlases and the development of algorithms dealing with big data. Semi-automatic segmentation technologies require interaction with the operator. They are used primarily for precise local segmentations, where only one organ or tissue is processed. In our previous work we used several techniques for adaptation of the once segmented reference human model to different individuals. This technique relies on anthropometric scaling, control points mapping and supervised segmentation [7, 8].

In the following two sections we discuss and present several methods for 3D reconstruction of vascular network and cardiac model from medical images.

2 VASCULAR SEGMENTATION

In the current work we consider two regions of interest: cerebral and coronary vessels. Input data is DICOM datasets obtained with contrast enhanced Computed Tomography Angiography

(ceCTA). For simplicity of presentation we assume that quasi-isotropic voxel sizes are used in this work.

Our automatic vessel segmentation methodology for coronary arteries was proposed in [9]. In the current work it is extended to process cerebral vessels. Essential steps of this method consist of aorta segmentation, computation of vesselness values, searching branches of aorta arch or ostia points, and removing segmentation errors near aorta boundary. Important additional step in the cerebral case is bone intensity decreasing by multiscale Match Mask Bone Elimintaion (multiscale MMBE) algorithm [10]. For every patient the last step requires not only ceCTA dataset but also corresponding CTA dataset not enhanced by contrast. All steps are shown in Figure 1.

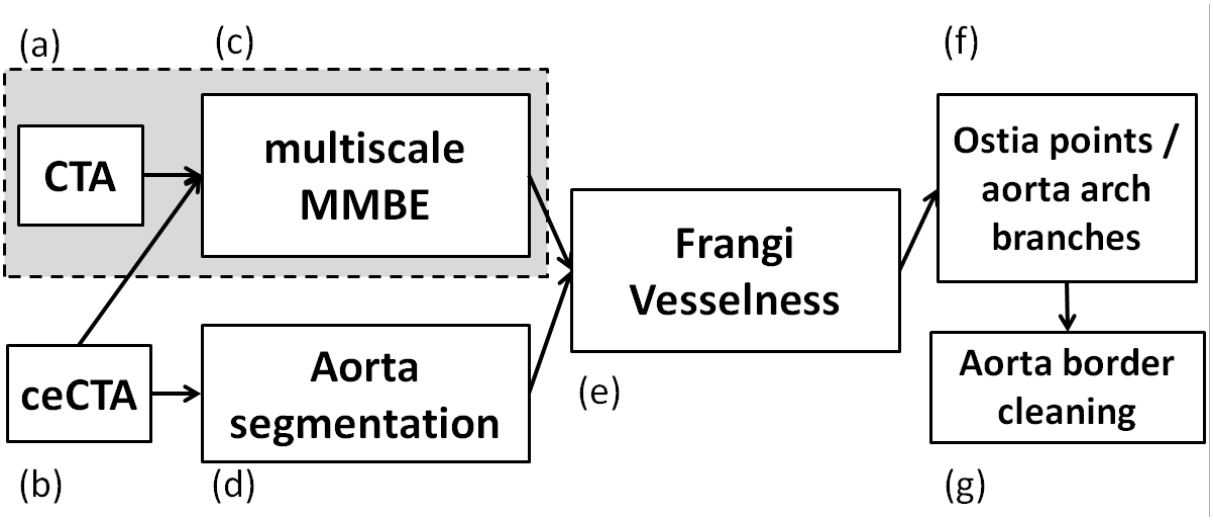

Figure 1: Segmentation pipeline. Gray rectangle highlights cerebral case only steps. (a) and (b) are algorithm inputs, (c)-(g) essential algorithm steps.

Large variation of vessel radii results in numerically expensive Hessian-based filtering. Since aorta is several times larger than arteries studied in this work it is natural to use specific algorithm for its segmentation. In both coronary and cerebral cases we perform the following steps. First, the Hough Circleness Transformation [11] is used to detect largest bright disk D corresponding to aorta cross-section. Second, connected mask is obtained by region growing, starting at the center of D, with lowest intensity inside of D as a threshold parameter. Third, IDT algorithm [1] cuts mask in bottlenecks and, finally, mathematical morphology operations are used to remove vessels branching from aorta.

Once aorta is segmented, the multiscale MMBE method is applied to decrease intensities of bone tissues in cerebral case. This approach allows us to apply standard segmentation methodologies to get anatomically correct segmentations.

The next step is computation of Frangi Vesselness [2], which results in bigger values inside bright tubular structures. In coronary datasets only coronary arteries and aorta represent these structures. In cerebral case such structures are bones and arteries, and once bones are darkened, Frangi Vesselness is applicable. Segmentation of arteries is produced by thresholding of vesselness values. Then coronary arteries and cerebral aorta arch branches are found as voxel connectivity components near the aorta boundary.

Final step is removal of segmentation errors. Thresholding of Frangi Vesselness values may produce “leaks” near the aorta boundary. Let us assume we have segmented object represented

by set of voxels A, but segmentation S contains set of extra voxels B, i.e. $S = A \cup B$. In case S is a connected component we call B as leak. In terms of definition leaks cannot be removed by "remove islands" procedure. Also leaks may have different shapes, so it is hard to find appropriate mathematical morphology operation to remove leaks automatically.

We propose automatic method for leaks removal from aorta boundary. Let us denote mask of cerebral vessels by V_{mask}, mask of aorta by A_{mask} and define voxel layer $L_i = \{v \in V_{\text{mask}} \mid \text{dist}(A_{\text{mask}}, v) = i\}$. For $i = i_{\max}, \ldots, 0$ the following procedure is taken: remove all voxels from layer L_i having no neighbouring voxels in L_{i+1}. Experiments has shown that $i_{\max}$ can be set to 15 voxels. In theory $i_{\max}$ must be set bigger than the thickness of a leak.

Several examples of vessel structure reconstruction are presented in [8, 9].

3 CARDIAC IMAGES SEGMENTATION

Mathematical modelling of electrophysiology requires an anatomical 3D cardiac model. Our group created a reference 3D cardiac model based of Visible Human Project (VHP) data [12]. This model is used for evaluation of modelling methods and algorithms. The reference model may be used for patient-specific adaptation in case medical imaging data is insufficient for complete segmentation.

Several segmentation techniques were examined for automatic segmentation of heart ventricles. The preprocessing steps include optional noise reduction using non-local means filtering and histogram equalization processing. The first used approach was based on SLIC supervoxel clustering [13] and recursive region adjacency graph partitioning.

The second approach was based on user-guided active contour segmentation with supervised random forest classification from ITK-SNAP segmentation platform [14]. The results of user-guided segmentation highly depend on user expertise.

Based on our experience we propose to combine both approaches: the supervised random forest classification is used for supervoxel grouping. Several post-processing steps are used to improve the segmentation.

VHP dataset provides CT, MRI and photo images of human cadaver. Transversal photo images are digitized with resolution 0.33×0.33 mm, distance between images is 1 mm. Photo images were aligned, rescaled and combined in a 3D volume dataset. ITK-SNAP segmentation software was used for visualization and segmentation. Only thorax region was investigated resulting in cropped image $573 \times 330 \times 170$ voxels with resolution 1 mm (Figure 2).

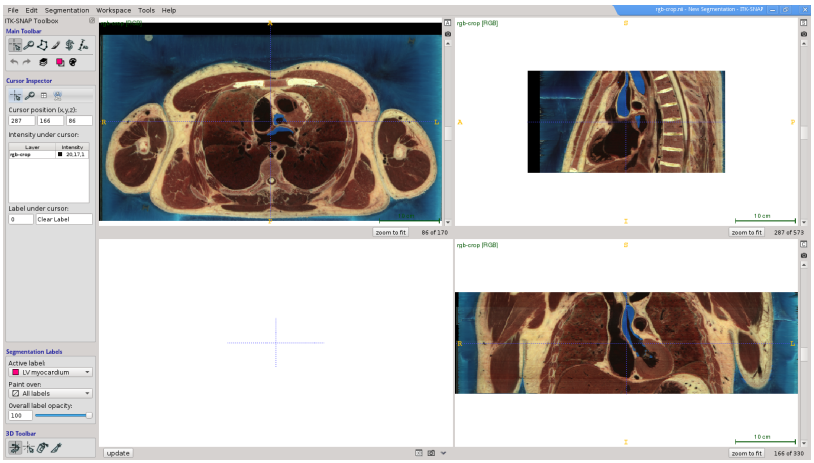

Figure 2: ITK-SNAP platform snapshot with VHP photo images of cardiac region.

Heart cavities and blood vessels were segmented using active contours method and random forest classifier. These regions are filled with blood and usually have a distinct color and/or intensity on photo images and CT/MRI images. The segmented region was split into parts corresponding to right atrium (RA), left atrium (LA), right ventricle (RV), left ventricle (LV), aorta, pulmonary trunk, superior vena cava and inferior vena cava (Figure 3).

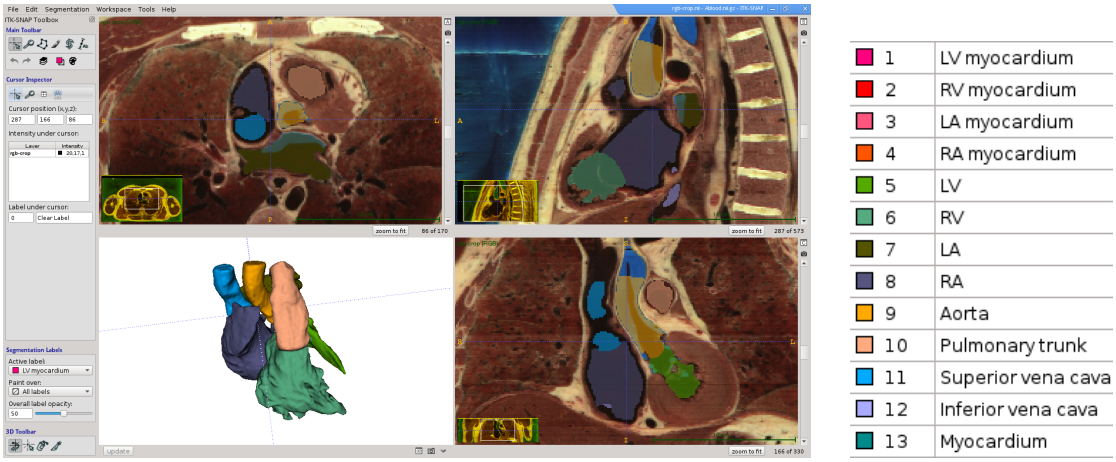

Figure 3: Segmentation of cardiac cavities and blood vessels.

Myocardium segmentation is performed in the vicinity of segmented heart cavities. Myocardium tissue differs in texture and intensity compared with neighbouring fat tissue, bones and lungs (Figure 4). This segmentation step is also performed using active contours method and random forest classifier.

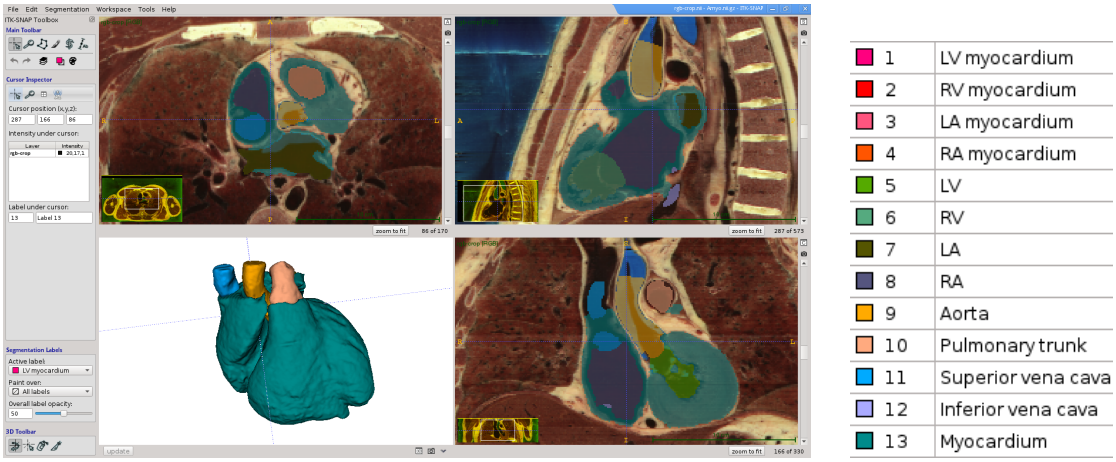

Figure 4: Myocardium segmentation.

The final step involves segmentation smoothing. The myocardium tissue was divided into four parts using mathematical morphology operations: right atrium, left atrium, right ventricle, and left ventricle (Figure 5). This division will be used in modelling algorithms for synthetic computation of myocardium fiber orientation.

The segmented model is a 3D structure with $128 \times 119 \times 129$ voxels with resolution 1 mm and 12 tissue labels corresponding to different heart cavities, blood vessels and four myocardium regions. The segmented model may be used for estimation of myocardium mass and ventricles

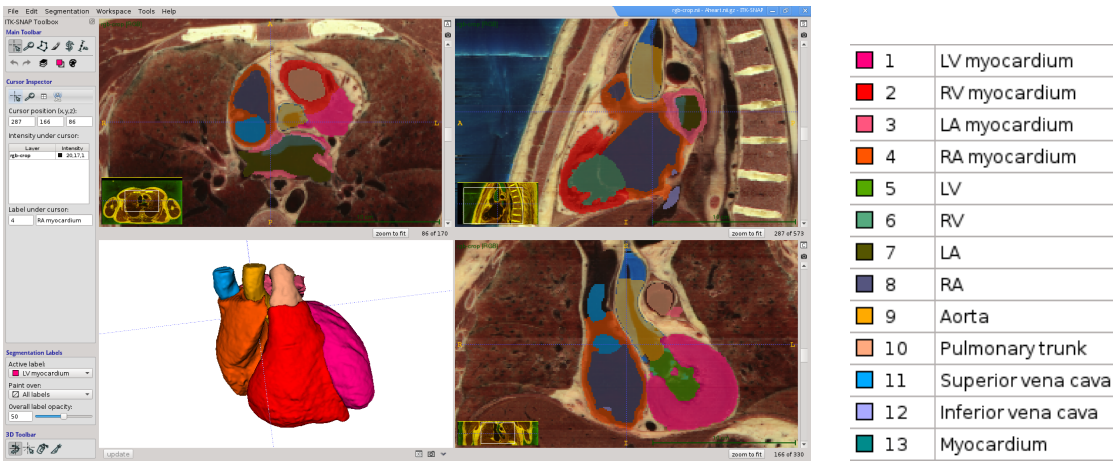

Figure 5: Final VHP segmented model.

volume. Assuming relative density of myocardium tissue is equal to 1.05 g/ml we obtain the mass of right ventricle 95 g, and left ventricle – 187 g. The volume of right ventricle is 77 ml, the volume of the left ventricle – 21 ml. The computed myocardium mass lies in reference limits for a male aged 38 years [15, 16]. We should note, that the volume of the left ventricle lies bellow the minimum reference values [16]. This inconsistency in ventricle volumes between VHP data and *in vivo* reference studies may be due to the stopped heart in VHP dataset. An underestimated volume of the left ventricle should be accounted in further investigations. The left ventricle volume may be extended by thickening the walls of left ventricle.

The adaptive unstructured tetrahedral mesh was constructed using Delaunay triangulation algorithm from CGAL Mesh library [17]. The maximum mesh size is 3 mm, the minimum mesh size in the vicinity of heart boundaries and material interfaces is 1 mm. The computational mesh consists of 367 318 tetrahedra and 77 953 vertices (Figure 6). Upscaling of multi-labeled segmented image was used to improve the resolution of input data.

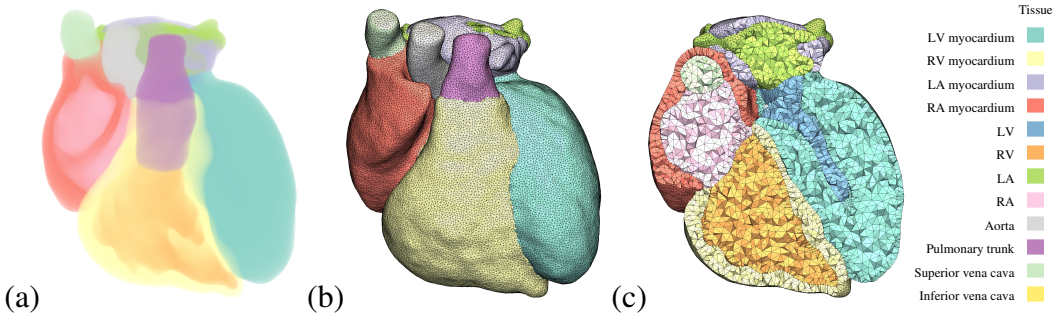

Figure 6: Unstructured mesh for VHP heart: (a) translucent 3D model; (b) triangular surface mesh; (c) volume cut of the tetrahedral mesh.

The cardiac mesh may be used in electrophysiology modelling. The proposed segmentation and mesh generation pipeline may be applied to patient's CT/MRI images.

4 CONCLUSIONS

The work addresses several segmentation techniques for generation of individualized computational domains on the basis of medical imaging datasets. Two algorithms were proposed for automatic vascular network segmentation and user-guided cardiac segmentation. Several

examples of numerical modeling applications are presented in [8, 9].

ACKNOWLEDGMENTS

The work was supported by the Russian Science Foundation (RSF) grant 14-31-00024.

REFERENCES

[1] L. Grady, Fast, quality, segmentation of large volumes – Isoperimetric distance trees. A. Leonardis, H. Bischof, A. Pinz eds. *Computer Vision – ECCV 2006*, Springer-Verlag, Berlin, Heidelberg, **3953**, 449–462, 2006.

[2] A.F. Frangi, W.J.Niessen, K.L. Vincken, M.A. Viergever, Multiscale vessel enhancement filtering. W.M. Wells, A. Colchester, S.L. Delp eds. *Medical Image Computing and Computer-Assisted Interventation – MICCAI'98*, Springer Verlag, Berlin, Germany, **1496**, 130–137, 1998.

[3] G. Lines, M. Buist, P. Grottum, et al., Mathematical models and numerical methods for the forward problem in cardiac electrophysiology. *Computing and Visualization in Science*, **5**, 215–239, 2002.

[4] M. Holtzman-Gazit, R. Kimmel, N. Peled, D. Goldsher, Segmentation of thin structures in volumetric medical images. *IEEE Transactions on Image Processing*, **15**, 354–363, 2006.

[5] A.G. Radaelli, J. Peiró, On the segmentation of vascular geometries from medical images. *International Journal for Numerical Methods in Biomedical Engineering*, **26**, 3–34, 2010.

[6] S.Y. Yeo, X. Xie, I. Sazonov, P. Nithiarasu, Segmentation of biomedical images using active contour model with robust image feature and shape prior. *International Journal for Numerical Methods in Biomedical Engineering*, **30**, 232–248, 2014.

[7] A.A. Danilov, D.V. Nikolaev, S.G. Rudnev, et al., Modelling of bioimpedance measurements: unstructured mesh application to real human anatomy. *Russian Journal of Numerical Analysis and Mathematical Modelling*, **27**, 431–440, 2012.

[8] Yu.V. Vassilevski, A.A. Danilov, T.M. Gamilov, et al., Patient-specific anatomical models in human physiology. *Russian Journal of Numerical Analysis and Mathematical Modelling*, **30**, 185–201, 2015.

[9] A. Danilov, Yu. Ivanov, R. Pryamonosov, Yu. Vassilevski, Methods of graph network reconstruction in personalized medicine. *International Journal for Numerical Methods in Biomedical Engineering*, doi: 10.1002/cnm.2754, 2015.

[10] H.A. Gratama van Andel, H.W. Venema, G.J. Streekstra, et al., Removal of bone in CT angiography by multiscale matched mask bone elimination. *Medical Physics*, **34**, 3711–3723, 2007.

[11] T.S. Yoo, M.J. Ackerman, W.E. Lorensen, et al., Engineering and algorithm design for an image processing API: A technical report on ITK – The Insight Toolkit. J.D. Westwood, et al. eds. *Proceedings of Medicine Meets Virtual Reality 02/10*, Amsterdam: IOS Press, 586–592, 2002.

[12] The National Library of Medicine's Visible Human Project, http://www.nlm.nih.gov/research/visible/.

[13] R. Achanta, A. Shaji, K. Smith, et al., SLIC superpixels compared to state-of-the-art superpixel methods. *IEEE Transactions on Pattern Analysis and Machine Intelligence*, **34**, 2274–2282, 2012.

[14] P.A. Yushkevich, J. Piven, H.C. Hazlett, et al., User-guided 3d active contour segmentation of anatomical structures: Significantly improved efficiency and reliability. *NeuroImage*, **31**, 1116–1128, 2006.

[15] A.M. Maceira, S.K. Prasad, M.Khan, D.J. Pennell, Reference right ventricular systolic and diastolic function normalized to age, gender and body surface area from steady-state free precession cardiovascular magnetic resonance. *European Heart Journal*, **27**, 2879–2888, 2006.

[16] P.A. Cain, R. Ahl, E. Hedstrom, et al., Age and gender specific normal values of left ventricular mass, volume and function for gradient echo magnetic resonance imaging: a cross sectional study. *BMC Medical Imaging*, **9**, doi: 10.1186/1471-2342-9-2, 2009.

[17] L. Rineau, M. Yvinec, A generic software design for delaunay refinement meshing. *Computational Geometry*, **38**, 100–110, 2007.